Graphical Abstract

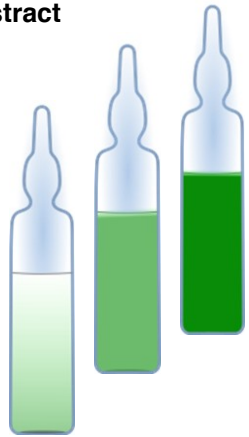

Dye quantification

HPLC-FLD quantification

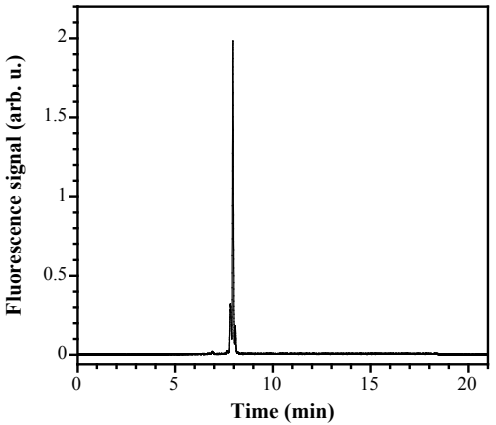

Optimization of formulation

Dye loading vs fluorescence

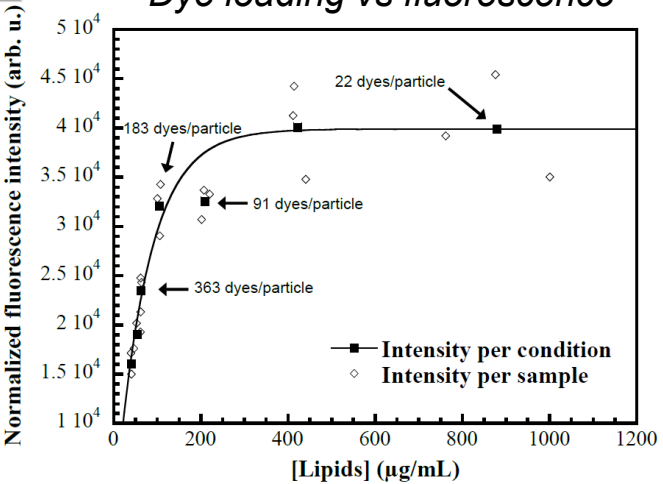

Selection of dye loading

Development and validation of an HPLC-fluorescence method for the quantification of IR780-oleyl dye in lipid nanoparticles

Mathieu Varache[1,2*], Marie Escudé[1,2], Corentin Laffont[1,2], Emilie Rustique[1,2], Anne-Claude Couffin[1,2*]

[1]*CEA-LETI, Microtechnologies for Biology and Healthcare Division, 17 rue des Martyrs, 38054 Grenoble Cedex 09, France*

[2]*Université Grenoble Alpes, 38000 Grenoble, France*

[*]Corresponding author: email's address: anne-claude.couffin@sfnano.fr, phone: +33 438 780 325, Fax: +33 438 785 787

Abstract

A reversed-phase (RP) high-performance liquid chromatography (HPLC) method for the content determination of IR780-oleyl (IRO) dye in lipid nanoparticles was developed and validated. Chromatographic separation was performed on a RP C18 column with a gradient program of water and acetonitrile both with 0.1% (v/v) TFA, at a flow rate of 1.0 mL/min and a total run of 21 min. IRO dye detection was made by fluorescence at emission wavelength of 773 nm (excitation wavelength: 744 nm). According to ICH guidelines, the developed method was shown to be specific, linear in the range 3-8 µg/mL (R^2=0.9998), precise at the intra-day and inter-day levels as reflected by the coefficient of variation (CV ≤ 1.98%) at three different concentrations (4, 6 and 8 µg/mL) and accurate, with recovery rates between 98.2-101.6% and 99.2-100.5%. The detection and quantitation limits were 0.41 and 1.24 µg/mL, respectively. Stability studies of sample processing showed that IRO dye was stable after 24 h in the autosampler or after three freeze/thaw cycles. Combined with fluorescence measurements, the developed method was successfully applied to optimize the loading capacity of IRO dye in the core of lipid nanoparticles.

Keywords:

Analytical method, fluorescence detection, lipid nanoparticles, high performance liquid chromatography, near infrared dye

1 Introduction

Throughout the last decade, bioimaging has become an essential modality to gain information on biological materials or processes, from subcellular structures to entire multicellular organisms. Amongst optical imaging modalities, fluorescence imaging has found particular interest because of its non-invasive and non-ionizing radiation limiting side effects, facilitates detection and monitoring of disease progression due to repeated observations (Etrych et al., 2016; Gibson et al., 2005). Many fluorescent dyes are currently employed to label tumors cells; either *in vivo* (in whole animal studies) or *in vitro*/*ex vivo*. In the near infrared (NIR) spectral region between 700 and 1000 nm, organisms and tissues possess low absorption and autofluorescence, thus enhancing deep tissue penetration and image sensitivity with limited background interference and photo-damage to biological samples. Consequently, fluorescent organic probes within the NIR spectral window can be readily detected and distinguished from the surrounding biological environment by commercially available imaging systems (Frangioni, 2003; Smith et al., 2009). Therefore, NIR fluorescence imaging is an attractive modality for *in vivo* cancer diagnosis and particularly used at the early stage of detection (Biffi et al., 2015; Santra et al., 2005). As an emerging field, many organic NIR probes have been designed with chemical structure based on cyanines, squaraine, phthalocyanines and porphyrin derivatives, or rhodamine and BODIPY analogues. These organic dyes have been prepared using different strategies including targeting activation and chemical conjugation; leading to improved chemical and photostability properties, as well as to increased fluorescence intensity and fluorescent half-life (Gibbs, 2012; Luo et al., 2011; Yi et al., 2014; Yuan et al., 2013). As NIR fluorescent light is suitable for real-time visualization in human surgery, different fluorescence imaging devices have become available for clinical studies and have been employed in the surgical management of patients (Gioux et al., 2010; Keereweer et al., 2011). Currently, the limitation of NIR fluorescence-guided surgery imaging is most likely due to

the limited availability of fluorophores with regulatory approval for human use (Alander et al., 2012; Mérian et al., 2012). IndoCyanine Green (ICG) being the only NIR dye which is approved by the US FDA (Food and Drug Administration), has been employed clinically in diagnosing metastases in a number of malignant conditions including breast, lung, skin and esophageal cancer (Hachey et al., 2016; Khullar et al., 2009; Troyan et al., 2009; van der Vorst et al., 2013; van Driel et al., 2014). The clinical development of such fluorophores is also hampered by intrinsic limitations *e.g.* poor hydrophilicity, quantum yield or instability *in vivo* (Achilefu, 2010; Frangioni, 2003; Hilderbrand and Weissleder, 2010). Taking into account the advantage of recent advances in the development of nanoparticles as drug delivery carriers, fluorescence probes have been encapsulated into nanoparticles or nanomaterials with the aim to improve its bioimaging applicability (Priem et al., 2015; Wittenberg and Haynes, 2009; Wolfbeis, 2015). This strategy has been successfully extended to newly designed NIR probes for tumor imaging and cancer diagnosis (Altinoğlu and Adair, 2010; Choi and Frangioni, 2010; He et al., 2010). NIR nanotracers are expected to preferentially accumulate into tumors driven by the EPR (Enhanced Permeability and Retention) effect allowing lesion localization and guiding surgeons to delineate tumor-free margins in intra-operative resection (Gibbs, 2012; Maeda, 2001). NIR nanoprobes, are currently in preclinical studies in glioma (Su et al., 2013), head and neck cancer (van Driel et al., 2014).

The iodide fluorophore IR780 exhibited suitable NIR optical properties with high photobrightening (Zhang et al., 2010a) and has been employed in sentinel lymph node “mapping” in animal and human studies (Yi et al., 2014; Zhang et al., 2010b). Moreover, IR780 has been used to design and deliver novel, multifunctional theranostic agents, via derivatization into micelles and its encapsulation into nanoparticles, for use in both imaging and photodynamic/thermal therapy (Jiang et al., 2015; Tan et al., 2012; Yuan et al., 2015; Yue et al., 2013).

Building on long-term development of lipid nanoparticle platform (Delmas et al., 2011; Goutayer et al., 2010; Lainé et al., 2014), we have formulated in 2013 a new lipid nanocarrier, loaded with modified IR780 dye (LipImage®815) for *in vivo* imaging. Studies in mice have demonstrated that

LipImage®815 displays prolonged circulation within the bloodstream and preferential accumulation within tumors; facilitating fluorescent imaging over 22 days after injection (Jacquart et al., 2013). The toxicity and biodistribution of LipImage®815 have been rapidly investigated in clinical trials (Phase 0/I) on healthy beagle dogs (Sayag et al., 2016). Recently, the potential of this agent as an *in vivo* NIR nanotracer has been evaluated for intraoperative fluorescence imaging in the surgical excision of malignant masses in dogs (Cabon et al., 2016). To facilitate potential clinical utility and regulatory approval, an extensive characterization of our Lipidot® platform has been undertaken with the development and validation of a large panel of analytical and physico-chemical methods (Varache et al., 2016).

As part of this work, we sought to develop and validate a High Performance Liquid Chromatographic Fluorescence Detection (HPLC-FLD) method for the quantification of IR780-oleyl (IRO) content in lipid nanoparticles, based on the recommendations of the International Conference on Harmonisation of Technical Requirements for Registration of Pharmaceuticals for Human Use; ICH guidelines Q2(R1)("ICH guideline Q2(R1) : Validation of Analytical Procedures : Text and Methodology," 2005). Using this HPLC-FLD method, we investigated the loading capacity and thus selected an optimal dye concentration of LipImage®815 for use in future fluorescence imaging guided-surgery applications.

2 Materials and methods

2.1 Materials

The IR780-oleyl dye (IRO) (purity: 98%) was prepared from reaction of IR780 iodide dye and oleylamine reagents, which are both commercially available. This synthesis was performed by Eras Labo (Saint-Nazaire-les-Eymes, France). Suppocire NB™ was purchased from Gattefossé S.A. (Saint-Priest, France). Myrj™ S40 (PEG 40 stearate, 1980 Da) and Super Refined™ Soybean Oil were obtained from Croda Uniquema (Chocques, France). Lipoid® S75 (soybean lecithin at 69% of phosphatidylcholine) was provided from Lipoid GmbH (Ludwigshafen, Germany). All

these excipients were pharmaceutical grade and used as received for preparing all formulations. Acetonitrile (ACN), absolute ethanol (EtOH), absolute methanol (MeOH), trifluoroacetic acid (TFA) 99.9% were supplied by Sigma Aldrich (Saint-Quentin-Fallavier, France). All other chemicals and reagents were analytical grade and were used without further purification. HPLC-grade water (specific resistance = 18.2 MΩ.cm) was obtained from a Classic DI MK2 water purification system (Elga, UK) and was used in all experiments. Lipid nanoparticles were formulated using a VCX750 Ultrasonic processor from Sonics (Newtown, USA) equipped with a 3 mm-diameter microtip. The balance was an XP105 from Mettler Toledo (Columbus, USA), the centrifuge was a Heraeus Pico 17 from Thermo Scientific (Waltham, USA) and the vortex was a Reax top from Heidolph (Schwabach, Germany).

2.2 Equipment and chromatographic conditions

A Waters Alliance 2695 Separation module equipped with a Waters 2475 fluorescence detector (FLD) and a Waters 186001863 column heater was used for IRO dye quantification. Chromatographic analysis was achieved on a C18 column (Sunfire^{TM}, 5 µm, 250 x 4.6 mm, 100 Å) (Waters, USA) at 30°C. Data analysis was acquired and processed using Empower^{TM} 2 software. A Waters Auto Purification LC/MS system, equipped with a 2545 Binary Gradient Module, a 515 HPLC pump, a 2767 Sample Manager, a 2998 Photodiode Array (PDA) detector and a 3100 mass detector, was used for identifying IRO dye components. LC/MS analysis was conducted using a C18 column (Atlantis T3, 5 µm, 250 x 4.6 mm, 100 Å) (Waters, USA) at room temperature. Mass spectrometric analysis was carried out in positive ionization electrospray mode with the following source conditions: capillary voltage 3.5 kV, cone voltage 35 V, source temperature 150°C, desolvation temperature 450°C, desolvation gas flow 900 L/h, and cone gas flow 50 L/h. The mass range m/z was fixed in the range 200-1000. Instrument control and data acquisition were performed using MassLynx SCN627 4.1 software. The optimized method used a binary gradient mobile phase consisting of (A) a mixture of water acidified with 0.1% (v/v) TFA solution and (B) a mixture of acetonitrile with 0.1% TFA solution. The gradient was applied as following: 0-5 min

from 50 to 98% solvent B; 5-10 min from 98 to 100% solvent B; 10-15 min 100% solvent B; 15-16 min from 100 to 50% solvent; 16-21 min 50% solvent B. A flow rate of 1 mL/min was used with a 20 µL injection volume. The eluted peaks were recorded at excitation and emission wavelengths of 744 and 773 nm, respectively. After optimization, the gain and emission unit full set of the Waters 2475 detector were respectively fixed at 1000 and 100. Separation conditions for LC/MS analysis were directly transferred from the procedure described above and applied without any modification.

2.3 Preparation of stock and standard solutions

Crude oil of IRO dye (10 mg) was dissolved in 100 mL of EtOH to prepare concentrated stock solution containing 100 µg /mL. From this later, one working standard solution (8 µg/mL) was obtained by further dilution of the stock solution with ethanol. For the preparation of linearity curve, calibration standards (3, 4, 5, 6, and 7 µg/mL) were prepared by further dilution of the standard solution at 8 µg/mL with ethanol.

2.4 Preparation of samples from lipid nanoparticle matrices

Before quantification, IRO dye has to be extracted from lipid nanoparticles by disintegrating the oil in water emulsion template. Typically, 200 µL of acetonitrile and 200 µL of methanol were added to 100 µL of dye-loaded lipid nanoparticles at 100 mg/mL of total lipids. The resulting mixture was vortexed and centrifuged at 16,200 g for 10 min. The supernatant was then collected and filtered through a 0.45-µm filter. Before quantifying the released dye using the developed method, the supernatant was diluted with ethanol, to reach suitable concentration in the linear range defined for the optimized method. For studying specificity, identical extractions conditions were applied to blank lipid nanoparticles (which were not loaded with IRO dye).

2.5 Method validation

The chromatographic method was validated in agreement with the ICH guidelines Q2(R1)("ICH guideline Q2(R1) : Validation of Analytical Procedures : Text and Methodology," 2005) in terms

of the following analytical parameters: specificity, linearity, accuracy, precision, range and robustness.

2.5.1 Specificity

The specificity was performed in order to determine the ability of the analytical method to measure the concentration of IRO dye into lipid nanoparticles without interferences due to substances that composed the nanoformulation (*e.g.* excipients included in nanoparticle formulation), buffer media or mobile phase components. In this way, specificity was evaluated by comparison of representative chromatograms containing possible interfering substances from lipid nanoformulations and samples containing IRO dye. The mobile phase signal was obtained by injecting an ethanol only blank sample.

2.5.2 Linearity and range

To evaluate linearity, calibration curves were prepared and analysed in triplicate. Linearity was determined by calculation of a regression linear line from the area vs. concentration plot for six standard solutions (3, 4, 5, 6, 7 and 8 µg/mL) using linear least squares methodology, and by analysis of the respective response factors (*i.e.* peak area divided by concentration of each standard sample).

2.5.3 Accuracy and precision

ICH guidelines recommend accuracy evaluation, using a minimum of nine determinations over a minimum of three levels covering the range specified. The accuracy and precision were determined over a period of 3 days using individually-prepared replicates (N=6) of quality control (QC) samples at three levels (4, 6 and 8 µg/mL), followed by their comparison with the calibration curves. The accuracy was expressed by (mean observed concentration/spiked concentration) x 100 and the precision by the coefficient of variation (CV = (standard deviation/mean) x 100). The concentration of each sample was determined using the calibration curve and analysed on the same day. QC samples were prepared as following: 100 µL of blank lipid nanoparticles (not loaded with

IRO dye) at 100 mg/mL of lipids were mixed with 200 µL of ACN and then 200 µL of IRO dye solution (at 40 µg/mL in MeOH) were spiked. The resulting mixtures were shaken and centrifuged as previously described above. QC samples at three different levels were obtained by appropriate dilution of the collected supernatant by using ethanol.

2.5.4 Detection and quantification limits

Limit of detection (LOD) and limit of quantification (LOQ) were calculated according to the following equations:

$$LOD = \frac{3.3\sigma}{S}$$

$$LOQ = \frac{10\sigma}{S}$$

where σ = standard deviation of the response, S = the slope of the calibration curve. σ and S were determined for a specific calibration curve obtained by analysing eight dye solutions from 0.1033 to 6.198 µg/mL.

2.5.5 Stability

Autosampler stability of IRO dye samples was assessed by maintaining the QC samples in the autosampler tray of the HPLC instrument for 24 h at room temperature (RT), protected from the light. Refresh-RT stability of the samples was obtained over three refresh-RT cycles, by thawing at RT for 2 h and refreshing (4°C) for 20 h. For each concentration and each storage condition, six replicates were analysed in one analytical batch. The stability of the compound was presented as the recovery (%) relative to the freshly prepared samples by comparing the peak area.

2.6 Preparation of dye-loaded lipid nanoparticles (LipImage® formulations)

2.6.1 Manufacturing of dye-loaded nanoparticles

LipImage®815 formulations were prepared according to our previous reported method (Delmas et al., 2011; Gravier et al., 2011; Jacquart et al., 2013). Briefly, an oil premix was prepared including,

respectively, 85, 255, and 65 mg of Soybean oil, Suppocire NC™, and Lipoid S75. In order to optimize the formulation, different amounts of dye (50, 100, 200, 400, 600, 800, and 1000 µL) dissolved in ethanol (10 mg/mL) were poured were into the lipid phase. As wax is in solid phase up to 35°C, the complete homogenization of oily phase has been carried out at liquid state by gently heating at 40°C without exceeding 50°C to avoid dye degradation. After complete evaporation of the solvent under argon flow, the continuous phase, composed of 345 mg of Myrj™ S40, and of the appropriate amount of aqueous medium (154 mM NaCl if not stated otherwise, qsp 2 mL) was introduced. The vial was then placed in a 20°C water bath and sonication cycles were performed during 20 min with intervals of 10 s "Pulse On" and 30 s "Pulse Off". Following filtration of the suspension (200 mg/mL of lipids) through a 5-µm cellulose Millipore membrane, purification was carried out overnight using dialysis (154 mM NaCl, MWCO: 12-14,000 Da, Spectra/Por®). Lipid nanoparticles were finally formulated at a theoretical total concentration of lipids of 100 mg/mL and then filtered through a 0.22-µm cellulose Millipore membrane for sterilization before characterization. Free-IRO dye nanoparticles were prepared by omitting dye loading. Characterizations of the nanoparticles were performed immediately. Sample preparations were performed in triplicate for each IRO dye concentration.

2.6.2 Particle size and size distribution

The hydrodynamic diameter of the particles was measured by Dynamic Light Scattering (DLS) at 173° angle using a Malvern Nano ZS instrument (Zeta Siser Nano ZS, Malvern Instruments, UK) equipped with a 4 mW He-Ne laser (λ = 532 nm). Lipid nanoparticle samples were diluted to 2 mg/mL of lipids in aqueous buffer (15.4 mM NaCl) and poured in Zeta Size Nano cells (Malvern Instruments) before each measurement, performed in triplicate. The mean particle size (Z-average diameter) was obtained from a fit of a single exponential to the correlation function with the corresponding polydispersity index (PDI). The plotted data represent mean values of N=3 independent measurements.

2.6.3 Determination of dye-loading and encapsulation efficiency

IRO dye content of nanoparticles was assessed after disintegration of the nanoparticles followed by collection and quantification of the supernatants obtained after centrifugation, as described in the sample preparation section. Each sample was prepared and analysed in duplicate. For each series of measurements, an IRO dye solution at 7.7 µg/mL was analysed to calculate the concentration of the unknown samples (the amount of entrapped dye). The number of dyes per nanoparticles and the local dye concentration were calculated by considering a particle diameter of 50 nm and a lipid density of 1.05 g/cm^3. Entrapment efficacy (EE) and dye loading (DL) were determined according to the following equations:

$$Entrapment\ efficiency\ (w/w) = \frac{Weight\ of\ loaded\ dye}{Weight\ of\ initially\ added\ dye} \text{ x } 100$$

$$Dye\ loading\ (w/w) = \frac{Weight\ of\ loaded\ dye}{Weight\ of\ loaded\ dye + weight\ of\ nanoparticles} \text{ x } 100$$

2.6.4 Photophysical properties

The absorbance measurements were performed in saline buffer (154 mM NaCl) using a Cary 300 Scan UV-Visible spectrophotometer (Varian, Les Ulis, France). The absorbance was measured at a total dye concentration of 0.456 µg/mL. Fluorescence intensities of the dilute samples were measured in duplicate using a microplate reader (TECAN Infinite M1000) at excitation and emission wavelengths of 793 and 814 nm, respectively. Results were expressed as the normalized fluorescence intensity (fluorescence intensity x $(1\text{-}10^{-0.1})/(1\text{-}10^{-absorbance})$) where the absorbance was determined for each sample at the maximum absorption wavelength, *i.e.* $\lambda = 793$ nm. Data normalization compensated for inhomogeneities within the samples, laser power fluctuations between measurements or coupling variations.

3 Results & Discussion

3.1 Development of the analytical method

3.1.1 Selection of an HPLC method with fluorescence detection

This is the first study to describe a simple, precise and accurate HPLC method coupled with fluorescence detection for the assessment of IRO dye derivatives encapsulated into nanomaterials (Fig. 1). The conventional method for quantitating IR780-iodide loaded into nanoparticles is by absorbance spectrophotometry at 780-800 nm after disruption of the nanosystems (Chen et al., 2016; Li et al., 2016; Pais-Silva et al., 2017; Peng et al., 2011). Whilst simple and rapid, it suffers from obvious low assay sensitivity. Furthermore, this assay is not specific, and quantitation of IR780-iodide by this method relies on the assumption that the dye is neither degraded nor transformed prior to analysis. Detection based on fluorescence modality should increase sensitivity, thus allowing precise quantification after administration in the whole-body volume and limiting the amount of sample required for this purpose. Furthermore, a quantitative method which meets the regulatory requirements is crucial to ensure the industrial transfer of our nanomedicine product. According to ICH guidelines and FDA guidance documents, a stability-indicating method must be chosen excluding UV-visible spectrophotometric assays (FDA, 2001, 2000; "ICH guideline Q2(R1) : Validation of Analytical Procedures : Text and Methodology," 2005). A stability-indicating method accurately measures variations within the active ingredients concentration, without interference from the others degradation products, impurities and excipients. HPLC is most widely used as analytical tool for the separation and quantification of the active pharmaceutical ingredients and their related substances. We, therefore, focused on FLD and HPLC for the development of our analytical method.

3.1.2 Sample preparation

When LipImage®815 formulation was initially developed, the content of the lipophilic-modified IR780, loaded into the core of the nanoparticles, was directly determined by measuring absorbance

values of particle suspension (Jacquart et al., 2013). As cyanine dyes, IRO dye exhibits lipophilic character fostering encapsulation or dissolution into fatty media (Gravier et al., 2011; Jacquart et al., 2013). Even if the loading of IRO dye into the core of the nanocarriers does not modify its optical properties, its quantification by HPLC relies on the detection of the individual species itself, regardless of all the excipients. Consequently, disintegration of dye-loaded nanoparticles followed by extraction of IRO dye from lipid matrices has been applied to release dye as free substance. This step was previously implemented by Guillot and co-workers (Guillot et al., 2015) for Cyclosporine A and was slightly modified for NIR dyes by adapting solvent nature and proportions. Considering the oil/water emulsion of lipid nanoparticles, methods involving hydro-organic solvents would destabilize the interface of droplets providing release of encapsulated entities and allowing surfactants to be solubilized. As IRO dye is highly soluble in MeOH, a disintegration step consists of mixing the nanoparticles with four volumes of ACN/MeOH:50/50 (v/v). Then, the supernatant is carefully collected and filtered after centrifugation. Before quantifying the released dye using the developed method, the supernatant is diluted with ethanol in order to reach suitable concentration in the linear range defined for the optimized method. Opaque containers or covering with aluminium foil was also employed to minimize light exposure.

3.1.3 Near infrared IRO dye derivatives as substances to be quantified

IR780-iodide dye and its derivatives have demonstrated suitable optical properties for *in vivo* bioimaging in the specific 700- 1000 nm wavelength window (Yuan et al., 2015; Zhang et al., 2010a, 2010b). To overcome the limitations of most of NIR dyes when injected in their free form in aqueous buffers (poor solubility, aggregations and strong adsorption on plasma proteins), novel nanoparticles have been employed as carriers (Pais-Silva et al., 2017). To facilitate efficient and prolonged encapsulation in the core of lipid nanoparticles, commercially available IR780-iodide dye has been derivatizated with an oleyl chain (C18 alkyl chain), enhancing its lipophilic character, to provide IR 780-Oleyl (IRO). The lipid nanoparticles encapsulating IRO dyes were annotated LipImage®815 as nanomedicine dedicated to *in vivo* imaging diagnosis (Jacquart et al.,

2013). The enhanced lipophilicity of IRO dye aims to foster a more deeply anchoring of dye into the core lipid of nanoparticle, preventing thereby its potential and prematurely escape outside the nanoparticles in the bloodstream before reaching tumor sites. The *in vivo* biodistribution pattern of IRO dye is modified by its encapsulation into nanoparticles. Free IRO is largely spread into liver and spleen organs after injection whereas a more homogeneous distribution in mice body is achieved for encapsulated IRO dye as well as a prolonged circulation in plasma (Jacquart et al., 2013). The IRO dye (Fig. 1(b)) was synthetized from a two-step chemical modification, as previously described (Jacquart et al., 2013). Initially, a carboxylic acid group was introduced in the fluorophore template. An oleyl chain was then grafted onto the dye using standard $–CO_2H/NH_2$ coupling chemistry, activated by (benzotriazol-1-yloxy)tris(dimethylamino)phosphonium hexafluorophosphate (BOP) and the addition of oleylamine. The solution of oleylamine reagent used for manufacturing desired IRO dye contained other amines with long fatty chains. Without prior separation of these amine analogues, substitution of chlorine groups of IR780 iodide molecules could occur in a same pattern as oleylamine. This finding has been evidenced by LC/MS analysis of manufactured IRO dye batch. MS chromatogram (total ion count, TIC) revealed a major peak (data not shown) with a molecular ion peak at m/z = 858.9 that can be assigned to the IRO dye with oleyl (C18:1) chain. MS chromatogram also showed two minor peaks with molecular ion peaks at m/z = 856.9 and 860.9 that can be attributed to the IR780 iodide dye with stearyl (C18:0) or linoleyl (C18:2) chains as lipid anchors. Under the selected HPLC-FLD conditions, the chromatogram of IRO dye batch (Fig. 2) shows three closed peaks: one major at 7.94 ± 0.01 min and two minors at 7.81 ± 0.01 and 8.06 ± 0.01 min, respectively. After peak integration processed between 7.5 and 8.3 min, these minor peaks represent (6.2 ± 0.2)% and (18.4 ± 0.2)% of the total peak area, while the major peak corresponds to (73.6 ± 0.2)%. Content of unwanted impurities are estimated to represent less than 2% of the total IRO dye batch. Considering low structural differentiation and similar lipophilic character of these C18-anchoring IR780 analogues, preparative separation technique cannot be applied due to obvious time-,

solvent- and dye-consuming considerations. Regarding optical properties in the NIR window, no significant modification would be anticipated, with such similar lipid anchoring. Consequently, IRO dye batch including three characterised C18-anchoring IR780 dyes was loaded to design LipImage®815 as nanoimaging agent. Integration of chromatograms was assessed between 7.5 and 8.3 min in order to take into account all the C18-anchoring IR780 analogues.

3.1.4 Method development and optimization

Because our modified IR780-iodide dye (IRO) possesses a high lipophilic character evidenced by log P = 12, and consequently high solubility in organic systems, chromatographic separation was performed on a RP18 column, and a binary gradient elution mobile phase consisting of: (A) a mixture of water acidified with 0.1% (v/v) TFA solution, and (B) a mixture of acetonitrile with 0.1% TFA solution was used. The lowest initial amount of solvent A (aqueous solvent) was found to be equal to 50% in order to prevent elution of the dye in the void volume of the column. Noticeable tailing and irregular shaping of IRO dye peaks were observed in isocratic mode whatever the proportions of the mobile phases. Poor and variable tailing factor values would have compromised the accuracy and precision of the method. Temperature was observed to not affect the elution and analysis was operated at 30°C to provide reproducibility. TFA solvent was used to avoid fluorescence instability due to pH variations. The excitation and emission wavelengths have been optimized by using the 3D scan mode in Empower. Finally, the detector was set to excite at 744 nm and measure the emission at 773 nm. Optimization of the gain and emission unit full set (EUFS) of the Waters 2475 detector was performed by the auto-optimizing gain and EUFS provided in the Empower software after which minor manual adjustments were made. Then the gain was fixed to 1000 whereas EUFS was levelled off at 100. As recommended by ICH guidelines, the system suitability was assessed by six replicate analyses of the dye at a concentration of 7.7 µg/mL. The %CV of peak area and retention time for IRO was found to be less than 1% (0.88% and 0.24%, respectively) indicating the suitability of the system. Under the

optimized conditions, the asymmetry factor for the major peak was reached 1.24 ± 0.09 (mean ± SD), which is acceptable value indicating good symmetry of the method.

3.2 Method validation

In our course of extensive characterization for industrial transfer, we have set out to investigate the validation of the proposed analytical HPLC-FLD method in order to prove its acceptability for intended IRO dye quantification. As recommended by the ICH guidelines ("ICH guideline Q2(R1) : Validation of Analytical Procedures : Text and Methodology," 2005), this validation included various studies such as specificity, linearity, precision and accuracy over three days, and stability.

3.2.1 Specificity

Specificity of the method was evaluated by comparing the chromatograms of IRO dyes with those of potential interfering formulation components. Supernatant of empty nanoparticles collected from the sample preparation protocol and a blank sample (ethanol) were analysed according to the proposed method and compared with the chromatogram of IRO dye containing samples (Fig. 3). The representative chromatograms of lipid nanoparticles containing IRO dye (C) and IRO dye solution (D), both with similar retention times, showed in both cases no interfering peaks. Additionally, no other peaks corresponding to any of the remaining components of the nanoparticle formulation or solvent can be observed in the chromatograms of blank nanoparticles (A) and the mobile phase (B). These data demonstrated the high specificity of the developed method.

3.2.2 Linearity

Linearity is defined as an interval in the measurement range of analytical method in which an output signal correlates linearly with the determined analyte concentration. For IRO dye, linearity was studied in the concentration range of 3-8 µg/mL by visual inspection of a calibration curve (Fig. 4(a)) and by calculating the regression equation and the correlation coefficient (R^2) by the

method of least squares. The slope and intercept were 12,199 ± 350 and 5,459 ± 1929, respectively. The correlation coefficient was 0.9998 ± 0.0004. The results indicate that good linearity was observed from 3.0 to 8.0 µg/mL since the regression coefficient $R^2 > 0.998$ is generally considered as evidence of acceptable fit of the data to the regression line (Shabir, 2003; Shabir et al., 2007). This suitable range was also demonstrated by plotting the relative responses (response factors) on Y-axis and the corresponding log concentrations on X-axis (Fig. 4(b)). Relative responses are in the range of 95% and 105% of the average value, thus reinforcing the evaluation of the method as linear (Sonnergaard, 2006). Poor linearity was observed while increasing the concentration until 16 µg/mL.

3.2.3 Detection and quantification limits

The lowest concentration at which an analyte can be detected (LOD) or quantified (LOQ) with acceptable precision and accuracy can be determined by different methodologies. In our study, these parameters have been calculated from the SD of the response and slope of a specific calibration curve obtained by injecting in triplicate 8 standards (concentrations from 0.1033 to 6.198 µg/mL). The calculated LOD of IRO dye was 0.41 µg/mL and the LOQ was 1.24 µg/mL. Although the analysis of the R^2 (0.998) determined by the method of least squares indicates an acceptable linearity, the study of the linear regression for the response factor at concentration levels between 0.1033 and 6.198 µg/mL (specific calibration curve) indicated poor linearity (linear regression slope: -759.48; RSD: 13.39%). It thus demonstrates that the correlation coefficient is not a true measure of linearity and should be reinforced by other linearity assessment method (Sonnergaard, 2006).

3.2.4 Accuracy and precision

Accuracy is defined by International Organization for Standardization (ISO) as “closeness of agreement between a measured quantity value and a true quantity value of a measurand”. Precision expresses closeness of agreement between a series of measurements from multiple sampling of the

same homogeneous sample under the prescribed conditions ("ICH guideline Q2(R1) : Validation of Analytical Procedures : Text and Methodology," 2005). Accuracy and precision were calculated at three concentration levels (4, 6 and 8 µg/mL) (Table 1). The intra-day and inter-day precision CV% was <2% at any concentration levels, thus indicating that the proposed method presents good precision. The intra-day and inter-day accuracy ranged between 98.2% and 101.6%, and between 99.2% and 100.5% (Table 1), thus showing strong agreement between experimental and theoretical values. According to FDA guidelines, accuracy should be 100 ± 2% and precision should not exceed 2% of the CV (G. Shabir, 2004; G. A. Shabir, 2004; Shabir et al., 2007). This analytical method was thus proved to be precise and accurate.

3.2.5 Stability

Stability studies of IRO dye samples indicated that the QC samples were stable in the auto-sampler for 24 h and after 1 or 3 cycles of refreshing-thawing since the recovery (%) relative to the freshly prepared samples are within the acceptance range of 90-110% (Kumar et al., 2014) (Table 2).

3.3 Applicability of the validated HPLC-FLD method: optimization of LipImage®815 formulation

As a nano-contrast agent, LipImage®815 has been designed for imaging purposes based on optical properties of entrapped dyes. For drug delivery purposes, the drug loading has to be as high as possible (typically 8-10% (w/w) up to 30% (w/w)) in order to deliver to the biological site a maximal dose of active molecules with lowest number of nanomaterials. For imaging, the NIR dye payload can be as low as 0.02 to 2.5 % (w/w). In our previous work, IRO dye was encapsulated in the core of the nanoparticles with a range between 0.07 and 0.7% (w/w) (Jacquart et al., 2013). In the present work, the dye payload was extended up to 1.3 % (w/w) in order to optimize LipImage®815 formulation. For each dye payload, three samples were formulated and then purified separately until the final product was obtained (at a lipid concentration of 100 mg/mL). For each sample, the concentration of IRO dye ($[Dye]^{exp}$) was determined using HPLC. Based on

these concentrations, the encapsulation efficiency (EE), the experimental dye loading (DL^{exp}) and the number of dyes per nanoparticle ($Dyes/NP^{exp}$) have been calculated by considering a particle diameter of 50 nm and a lipid density of 1.05 g/cm^3 (Table 3). By plotting the theoretical dye loading (DL^{theo}) versus the experimental dye loading (DL^{exp}), we are able to show the entrapment evolution over the selected range of dye loading (Fig. 5). As previously observed (Jacquart et al., 2013), loading of the IRO dye in the core of the nanoparticle is highly efficient (80 < EE < 90 %) even with the highest number of dyes per nanoparticle (>85% yield, up to 476 dyes/nanoparticle). As previously observed for other cyanine dyes, the presence of the alkyl C18 lipophilic chains on its structure ensures encapsulation into the lipid core (Gravier et al., 2011). Although EE values are high, they pointed out a loss of raw materials (~15-20%), which occurs during the nanoparticles manufacturing. Unfortunately, analytical methods for lipid quantification are not yet developed and validated to investigate raw material loss. However, using the developed HPLC method, we attempted to identify the limiting steps resulting in loss of dye as raw materials. The nanoparticles are produced through three main steps: i) preparation of aqueous and oily phases including loading of dye, ii) formulation of lipid nanoparticles by emulsification using ultrasonication, iii) purification of nanoparticles using dialysis technique. Before dialysis, nanoparticle suspensions are filtered through a 5-µm cellulose membrane to remove large aggregates such as excipients (soybean oil and wax) which are not included in the nanoparticle formulation. Using our validated method, the concentrations of IRO dye for two suspensions with DL^{theo} of 0.79% (w/w) were measured before and after the 5-µm filtration step. We determined that EE decreased from (99.4 ± 2.2)% to (94.6 ± 1.0)% with the 5-µm filtration (data not shown). Consequently, the filtration step before dialysis removes dye, which has been solubilised in the fatty media (soybean and wax) but not integrated in the particle formulation. It was also, however, evident that filtration performed after dialysis (through a 0.22-µm cellulose membrane to ensure sterility) does not remove dye. Indeed, EE remained almost constant (not shown) after this filtration step (EE = 94.9 ± 2.1% before and 94.2 ± 2.0% after filtration). Diffusion Light

Scattering (DLS) was also used to assess LipImage®815 hydrodynamic diameter and polydispersity index. As previously demonstrated on a narrower range of dye loading (Jacquart et al., 2013), both hydrodynamic diameter (Z-average diameter) and polydispersity index (PDI) were unaffected by dye loading (Fig. 6). For *in vivo* imaging applications, fluorescence intensity has to be as high as possible while the amount of nanomaterials as low as possible. Also, the dye loading can also affect the fluorescence intensity due to the nano-confinement. For this reason, we have studied the fluorescence intensity of the suspensions as a function of dye loading. In order to minimise re-absorption effects in the fluorescence measurements, the total IRO dye concentration of each sample was adjusted (to provide absorbance values <0.1 at the excitation wavelength) (Dhami et al., 1995). Above this level, non-linear effects may be observed due to inner filter effects, and thereby the resulting fluorescence intensity may be perturbed. Thanks to the concentration of IRO dye ($[Dye]^{exp}$) determined using our validated HPLC-FLD method, each sample was suitably diluted with buffer saline solution (154 mM NaCl) until a final dye concentration of 0.456 µg/mL, limiting high concentration effect, as checked by absorbance values measured below 0.1. Normalized fluorescence intensity has been plotted against the number of IRO dyes per nanoparticle (Fig. 7). Normalized fluorescence intensity linearly decreases as a function of the experimental number of dyes entrapped in the nanoparticle core. This may be explained by the well-known self-quenching caused by the dye proximity when dye loading increased, leading to energy transfer between dyes (Shimizu et al., 2014; West and Pearce, 1965; Zhegalova et al., 2014). The normalized fluorescence intensity has been also expressed in function of the lipid concentration (*i.e.* the number of particles) after diluting the samples to reach an IRO dye concentration of 0.456 µg/mL (Fig. 8). Above 91 dyes/particle (when the number of particles decreases), the normalized fluorescence intensity drastically decreases while the dye loading increased. Fluorescence intensity remains almost constant below 91 dyes/particle even if the dye loading decreases (the number of particles increases). This supports the work of Gravier and co-workers (Gravier et al., 2011), who demonstrated for 50 nm sized lipid nanoparticles loaded with

DiD that the self-quenching value appears when internal concentration reaches above 200 dyes/particle. Within the range of internal concentration between 22 and 91 dyes/particle, we thus possess nanoparticle suspensions with similar fluorescence properties which differ in nanoparticle concentration. A sample is either composed of 22 dyes/particle with a large number of nanoparticles ([Lipids] = 800 µg/mL) or 91 dyes/particle with a lower amount of nanoparticles ([Lipids] = 210 µg/mL). As lipid nanoparticles are considered as carriers without imaging ability, the lowest amount is injected in the body, the best safety is expected (or the undesired effects are limited). Then, the formulation composed of 91 dyes/particle was selected for further preclinical studies (Cabon et al., 2016; Sayag et al., 2016).

4 Conclusion

We have developed a simple, accurate and validated reversed-phase HPLC-FLD method for the quantification of IR780-oleyl content in lipid nanoparticles according to ICH guidelines. This method is particularly relevant since the quantification of NIR dyes traditionally is undertaken via absorbance, which may be affected by impurities, degradation and/or biotransformation products. This HPLC-FLD method is currently useful for the routine dye analysis at laboratory scale and could be easily applied with slight modifications to the quantification of other NIR dyes such as lipophilic DiD, DiO, DiI cyanine dyes for developing new NIR nanoproducts. Meeting regulatory requirements, this fast and simple method could be used for In Process Control (IPC) strategy to estimate variations of IRO dye concentrations, which can occur during the manufacturing process of LipImage®815. This HPLC-FLD method represents a starting point to design a complete analytical method for the analysis of biological samples during clinical evaluation.

Acknowledgement

This work was financially supported by BpI France and is part of the NICE project aiming to foster the clinical and industrial development of nanomedicine products.

Figures caption

Figure 1: LipImage®815 schematic representation. (a) LipImage are dye-loaded oily droplets dispersed in buffer solution (NaCl, 154 mM). Their fluorescent properties are conferred by IRO dye (b), encapsulated in the lipid core and/or the surfactant layer.

Figure 2: Representative chromatogram between 7 and 9 min of IRO dye solution (8 µg/mL).

Figure 3: Representative chromatograms corresponding to (A) blank lipid nanoparticles, (B) mobile phase signal, (C) IRO-loaded lipid nanoparticles, and (D) IRO dye solution (8 µg/mL). Chromatograms are presented between a) 0 – 21 min and b) 7 – 9 min.

Figure 4: Linearity studies for the proposed HPLC method: (a) calibration curve obtained with IRO dye solutions (n=18 per days), and (b) relative responses (response factors) versus IRO concentration. Data are mean of calibration curve performed on three consecutive days.

Figure 5: Encapsulation range of the IRO dye into nanoparticles.

Figure 6: Mean hydrodynamic diameter (Z-average diameter) and Polydispersity index (PDI) obtained for selected encapsulation range of IRO dye. Results are expressed as average and SD of three independent samples analysed in triplicate.

Figure 7: Normalized fluorescence intensity against the number of IRO molecules per nanoparticle. For each sample, IRO dye concentration was adjusted at 0.456 µg/mL.

Figure 8: Normalized fluorescence intensity against the lipid concentration. For each sample, IRO dye concentration was adjusted at 0.456 μg/mL.

Tables

Table 1: Intra- and inter-day accuracy and precision of HPLC-FLD assay for IRO dye. Spiked recovery method was used for accuracy.

		Accuracy and precision of QC samples			
		Day 1 (n=6)	**Day 2 (n=6)**	**Day 3 (n=6)**	**Overall (n=18)**
4.0 µg/mL	Mean	4.06	3.95	3.98	3.99
	S.D.	0.08	0.07	0.08	0.08
	CV (%)	1.98	1.66	1.91	1.95
	Recovery (%)	101.5	98.8	99.5	99.9
6.0 µg/mL	Mean	6.09	6.07	5.92	6.03
	S.D.	0.05	0.06	0.08	0.10
	CV (%)	0.80	0.99	1.53	1.72
	Recovery (%)	101.6	101.3	98.6	100.5
8.0 µg/mL	Mean	7.95	8.01	7.86	7.94
	S.D.	0.10	0.13	0.12	0.12
	CV (%)	1.27	1.66	1.59	1.53
	Recovery (%)	99.3	100.1	98.2	99.2

Table 2: Stability of IRO dye QC samples determined with replicates (n = 6) for each concentration. [a]Stability in the autosampler was performed at room temperature, [b]one cycle of refreshing-thawing, [c]three cycles of refreshing-thawing

Nominal	**24 h in the**	**Post-**	**Post-**

concentration (µg/mL)	autosampler[a] (%)	preparation 1 cycle[b] (%)	preparation 3 cycles[c] (%)
4.0	101.4 ± 4.3	101.4 ± 2.4	100.7 ± 3.3
6.0	100.8 ± 3.2	100.7 ± 3.4	99.8 ± 2.1
8.0	99.9.4 ± 3.5	100.7 ± 3.1	100.5 ± 2.4

Table 3: Concentration of IRO dye for a concentration of lipids at 100 mg/mL, number of dyes per nanoparticle (NP), dye loading (DL) and entrapment efficiency (EE). For each concentration, results are expressed as average and SD of three independent samples analysed in duplicate. The number of IRO dyes per nanoparticle was calculated from the concentration of dye measured on the final product and by considering a particle diameter of 50 nm and a lipid density of 1.05 g/cm^3.

$[Dye]^{theo}$ (µg/mL)	DL^{theo} (%)	$[Dye]^{exp}$ (µg/mL)	DL^{exp} (%)	EE (%)	$Dyes/NP^{exp}$
67	0.07	52.5 ± 6.4	0.052 ± 0.006	78.6 ± 9.4	22.0 ± 2.7
133	0.13	108.1 ± 4.1	0.108 ± 0.004	81.0 ± 2.9	45.4 ± 1.7
267	0.27	217.8 ± 10.9	0.217 ± 0.011	81.7 ± 4.0	91.4 ± 4.6
533	0.53	436.5 ± 50.5	0.43 ± 0.050	82.1 ± 9.6	183.2 ± 21.2
798	0.79	728.8 ± 16.2	0.723 ± 0.016	91.6 ± 1.9	305.8 ± 6.8
1,060	1.04	925.1 ± 66.1	0.855 ± 0.108	87.3 ± 6.1	362.5 ± 45.7
1,322	1.31	1,133.4 ± 20.5	1.119 ± 0.020	85.5 ± 1.6	475.6 ± 8.6

References

Achilefu, S., 2010. The Insatiable Quest for Near Infrared Fluorescent Probes for Molecular Imaging. Angew. Chem. Int. Ed Engl. 49, 9816–9818. doi:10.1002/anie.201005684

Alander, J.T., Kaartinen, I., Laakso, A., Pätilä, T., Spillmann, T., Tuchin, V.V., Venermo, M.,

Välisuo, P., 2012. A review of indocyanine green fluorescent imaging in surgery. Int. J. Biomed. Imaging 2012, 940585. doi:10.1155/2012/940585

Altinoğlu, E.I., Adair, J.H., 2010. Near infrared imaging with nanoparticles. Wiley Interdiscip. Rev. Nanomed. Nanobiotechnol. 2, 461–477. doi:10.1002/wnan.77

Biffi, S., Voltan, R., Rampazzo, E., Prodi, L., Zauli, G., Secchiero, P., 2015. Applications of nanoparticles in cancer medicine and beyond: optical and multimodal in vivo imaging, tissue targeting and drug delivery. Expert Opin. Drug Deliv. 12, 1837–1849. doi:10.1517/17425247.2015.1071791

Cabon, Q., Sayag, D., Texier, I., Navarro, F., Boisgard, R., Virieux-Watrelot, D., Ponce, F., Carozzo, C., 2016. Evaluation of intraoperative fluorescence imaging-guided surgery in cancer-bearing dogs: A prospective proof-of-concept phase II study in 9 cases. Transl. Res. 170, 73–88. doi:10.1016/j.trsl.2015.12.001

Chen, Y., Li, Z., Wang, H., Wang, Y., Han, H., Jin, Q., Ji, J., 2016. IR-780 Loaded Phospholipid Mimicking Homopolymeric Micelles for Near-IR Imaging and Photothermal Therapy of Pancreatic Cancer. ACS Appl. Mater. Interfaces 8, 6852–6858. doi:10.1021/acsami.6b00251

Choi, H.S., Frangioni, J.V., 2010. Nanoparticles for biomedical imaging: fundamentals of clinical translation. Mol. Imaging 9, 291–310.

Delmas, T., Couffin, A.-C., Bayle, P.A., de Crécy, F., Neumann, E., Vinet, F., Bardet, M., Bibette, J., Texier, I., 2011. Preparation and characterization of highly stable lipid nanoparticles with amorphous core of tuneable viscosity. J. Colloid Interface Sci. 360, 471–481. doi:10.1016/j.jcis.2011.04.080

Dhami, S., Mello, A.J.D., Rumbles, G., Bishop, S.M., Phillips, D., Beeby, A., 1995. Phthalocyanine Fluorescence at High Concentration: Dimers or Reabsorption Effect? Photochem. Photobiol. 61, 341–346. doi:10.1111/j.1751-1097.1995.tb08619.x

Etrych, T., Lucas, H., Janoušková, O., Chytil, P., Mueller, T., Mäder, K., 2016. Fluorescence optical imaging in anticancer drug delivery. J. Controlled Release 226, 168–181. doi:10.1016/j.jconrel.2016.02.022

FDA, 2001. Guidance for Industry: Bioanalytical Method Validation.

FDA, 2000. Guidance for Industry: Analytical Procedures and Methods Validation.

Frangioni, J.V., 2003. In vivo near-infrared fluorescence imaging. Curr. Opin. Chem. Biol. 7, 626–634.

Gibbs, S.L., 2012. Near infrared fluorescence for image-guided surgery. Quant. Imaging Med. Surg. 2, 177–187.

Gibson, A.P., Hebden, J.C., Arridge, S.R., 2005. Recent advances in diffuse optical imaging. Phys. Med. Biol. 50, R1. doi:10.1088/0031-9155/50/4/R01

Gioux, S., Choi, H.S., Frangioni, J.V., 2010. Image-guided surgery using invisible near-infrared light: fundamentals of clinical translation. Mol. Imaging 9, 237–255.

Goutayer, M., Dufort, S., Josserand, V., Royère, A., Heinrich, E., Vinet, F., Bibette, J., Coll, J.-L., Texier, I., 2010. Tumor targeting of functionalized lipid nanoparticles: Assessment by in vivo fluorescence imaging. Eur. J. Pharm. Biopharm. 75, 137–147. doi:10.1016/j.ejpb.2010.02.007

Gravier, J., Navarro, F.P., Delmas, T., Mittler, F., Couffin, A.-C., Vinet, F., Texier, I., 2011. Lipidots: competitive organic alternative to quantum dots for in vivo fluorescence imaging. J. Biomed. Opt. 16, 096013. doi:10.1117/1.3625405

Guillot, A., Couffin, A.-C., Sejean, X., Navarro, F., Limberger, M., Lehr, C.-M., 2015. Solid Phase Extraction as an Innovative Separation Method for Measuring Free and Entrapped Drug in Lipid Nanoparticles. Pharm. Res. 32, 3999–4009. doi:10.1007/s11095-015-1761-8

Hachey, K.J., Gilmore, D.M., Armstrong, K.W., Harris, S.E., Hornick, J.L., Colson, Y.L., Wee, J.O., 2016. Safety and feasibility of near-infrared image-guided lymphatic mapping of regional lymph nodes in esophageal cancer. J. Thorac. Cardiovasc. Surg. 152, 546–554. doi:10.1016/j.jtcvs.2016.04.025

He, X., Gao, J., Gambhir, S.S., Cheng, Z., 2010. Near-infrared fluorescent nanoprobes for cancer molecular imaging: status and challenges. Trends Mol. Med. 16, 574–583. doi:10.1016/j.molmed.2010.08.006

Hilderbrand, S.A., Weissleder, R., 2010. Near-infrared fluorescence: application to in vivo molecular imaging. Curr. Opin. Chem. Biol. 14, 71–79. doi:10.1016/j.cbpa.2009.09.029

ICH guideline Q2(R1) : Validation of Analytical Procedures : Text and Methodology, 2005.

Jacquart, A., Kéramidas, M., Vollaire, J., Boisgard, R., Pottier, G., Rustique, E., Mittler, F., Navarro, F.P., Boutet, J., Coll, J.-L., Texier, I., 2013. LipImage™ 815: Novel dye-loaded lipid nanoparticles for long-term and sensitive in vivo near-infrared fluorescence imaging. J. Biomed. Opt. 18. doi:10.1117/1.JBO.18.10.101311

Jiang, C., Cheng, H., Yuan, A., Tang, X., Wu, J., Hu, Y., 2015. Hydrophobic IR780 encapsulated in biodegradable human serum albumin nanoparticles for photothermal and photodynamic

therapy. Acta Biomater. 14, 61–69. doi:10.1016/j.actbio.2014.11.041

Keereweer, S., Kerrebijn, J.D.F., van Driel, P.B.A.A., Xie, B., Kaijzel, E.L., Snoeks, T.J.A., Que, I., Hutteman, M., van der Vorst, J.R., Mieog, J.S.D., Vahrmeijer, A.L., van de Velde, C.J.H., Baatenburg de Jong, R.J., Löwik, C.W.G.M., 2011. Optical image-guided surgery--where do we stand? Mol. Imaging Biol. MIB Off. Publ. Acad. Mol. Imaging 13, 199–207. doi:10.1007/s11307-010-0373-2

Khullar, O., Frangioni, J.V., Grinstaff, M., Colson, Y.L., 2009. Image-guided sentinel lymph node mapping and nanotechnology-based nodal treatment in lung cancer using invisible near-infrared fluorescent light. Semin. Thorac. Cardiovasc. Surg. 21, 309–315. doi:10.1053/j.semtcvs.2009.11.009

Kumar, M., Sharma, G., Singla, D., Singh, S., Sahwney, S., Chauhan, A.S., Singh, G., Kaur, I.P., 2014. Development of a validated UPLC method for simultaneous estimation of both free and entrapped (in solid lipid nanoparticles) all-trans retinoic acid and cholecalciferol (vitamin D3) and its pharmacokinetic applicability in rats. J. Pharm. Biomed. Anal. 91, 73–80. doi:10.1016/j.jpba.2013.12.011

Lainé, A.-L., Gravier, J., Henry, M., Sancey, L., Béjaud, J., Pancani, E., Wiber, M., Texier, I., Coll, J.-L., Benoit, J.-P., Passirani, C., 2014. Conventional versus stealth lipid nanoparticles: Formulation and in vivo fate prediction through FRET monitoring. J. Controlled Release 188, 1–8. doi:10.1016/j.jconrel.2014.05.042

Li, Z., Wang, H., Chen, Y., Wang, Y., Li, H., Han, H., Chen, T., Jin, Q., Ji, J., 2016. pH- and NIR Light-Responsive Polymeric Prodrug Micelles for Hyperthermia-Assisted Site-Specific Chemotherapy to Reverse Drug Resistance in Cancer Treatment. Small 12, 2731–2740. doi:10.1002/smll.201600365

Luo, S., Zhang, E., Su, Y., Cheng, T., Shi, C., 2011. A review of NIR dyes in cancer targeting and imaging. Biomaterials 32, 7127–7138. doi:10.1016/j.biomaterials.2011.06.024

Maeda, H., 2001. The enhanced permeability and retention (EPR) effect in tumor vasculature: the key role of tumor-selective macromolecular drug targeting. Adv. Enzyme Regul. 41, 189 – 207. doi:10.1016/S0065-2571(00)00013-3

Mérian, J., Gravier, J., Navarro, F., Texier, I., 2012. Fluorescent Nanoprobes Dedicated to in Vivo Imaging: From Preclinical Validations to Clinical Translation. Molecules 17, 5564–5591. doi:10.3390/molecules17055564

Pais-Silva, C., de Melo-Diogo, D., Correia, I.J., 2017. IR780-loaded TPGS-TOS micelles for breast cancer photodynamic therapy. Eur. J. Pharm. Biopharm. 113, 108–117. doi:10.1016/j.ejpb.2017.01.002

Peng, X., Wang, Y., Huang, D., Wang, Y., Shin, H.J., Chen, Z., Spewak, M., Mao, H., Wang, X., Wang, Y., Chen, Z. (Georgia), Nie, S., Shin, D.M., 2011. Targeted Delivery of Cisplatin to Lung Cancer Using ScFvEGFR-Heparin-Cisplatin Nanoparticles. ACS Nano 5, 9480–9493. doi:10.1021/nn202410f

Priem, B., Tian, C., Tang, J., Zhao, Y., Mulder, W.J.M., 2015. Fluorescent nanoparticles for the accurate detection of drug delivery. Expert Opin. Drug Deliv. 12, 1881–1894. doi:10.1517/17425247.2015.1074567

Santra, S., Dutta, D., Walter, G.A., Moudgil, B.M., 2005. Fluorescent Nanoparticle Probes for Cancer Imaging. Technol. Cancer Res. Treat. 4, 593–602. doi:10.1177/153303460500400603

Sayag, D., Cabon, Q., Texier, I., Navarro, F.P., Boisgard, R., Virieux-Watrelot, D., Carozzo, C., Ponce, F., 2016. Phase-0/phase-I study of dye-loaded lipid nanoparticles for near-infrared fluorescence imaging in healthy dogs. Eur. J. Pharm. Biopharm. 100, 85–93. doi:10.1016/j.ejpb.2016.01.001

Shabir, G., 2004. Step-by-step analytical methods and protocol in the quality system compliance industry. J. Valid. Technol. 314–24.

Shabir, G.A., 2004. A practical approach to validation of HPLC methods under current good manufacturing practices. J. Valid. Technol. 10, 210–218.

Shabir, G.A., 2003. Validation of high-performance liquid chromatography methods for pharmaceutical analysis. Understanding the differences and similarities between validation requirements of the US Food and Drug Administration, the US Pharmacopeia and the International Conference on Harmonization. J. Chromatogr. A 987, 57–66.

Shabir, G.A., Lough, W.J., Arain, S.A., Bradshaw, T.K., 2007. Evaluation and Application of Best Practice in Analytical Method Validation. J. Liq. Chromatogr. Relat. Technol. 30, 311–333. doi:10.1080/10826070601084753

Shimizu, Y., Temma, T., Hara, I., Makino, A., Yamahara, R., Ozeki, E., Ono, M., Saji, H., 2014. Micelle-based activatable probe for in vivo near-infrared optical imaging of cancer biomolecules. Nanomedicine Nanotechnol. Biol. Med. 10, 187–195. doi:10.1016/j.nano.2013.06.009

Smith, A.M., Mancini, M.C., Nie, S., 2009. Bioimaging: Second window for in vivo imaging. Nat. Nanotechnol. 4, 710–711. doi:10.1038/nnano.2009.326

Sonnergaard, J.M., 2006. On the misinterpretation of the correlation coefficient in pharmaceutical sciences. Int. J. Pharm. 321, 12–17. doi:10.1016/j.ijpharm.2006.06.001

Su, X., Cheng, K., Wang, C., Xing, L., Wu, H., Cheng, Z., 2013. Image-guided resection of malignant gliomas using fluorescent nanoparticles. Wiley Interdiscip. Rev. Nanomed. Nanobiotechnol. 5, 219–232. doi:10.1002/wnan.1212

Tan, X., Luo, S., Wang, D., Su, Y., Cheng, T., Shi, C., 2012. A NIR heptamethine dye with intrinsic cancer targeting, imaging and photosensitizing properties. Biomaterials 33, 2230–2239. doi:10.1016/j.biomaterials.2011.11.081

Troyan, S.L., Kianzad, V., Gibbs-Strauss, S.L., Gioux, S., Matsui, A., Oketokoun, R., Ngo, L., Khamene, A., Azar, F., Frangioni, J.V., 2009. The FLARE^{TM} Intraoperative Near-Infrared Fluorescence Imaging System: A First-in-Human Clinical Trial in Breast Cancer Sentinel Lymph Node Mapping. Ann. Surg. Oncol. 16, 2943–2952. doi:10.1245/s10434-009-0594-2

van der Vorst, J.R., Schaafsma, B.E., Verbeek, F.P.R., Swijnenburg, R.J., Hutteman, M., Liefers, G.J., van de Velde, C.J.H., Frangioni, J.V., Vahrmeijer, A.L., 2013. Dose optimization for near-infrared fluorescence sentinel lymph node mapping in patients with melanoma. Br. J. Dermatol. 168, 93–98. doi:10.1111/bjd.12059

van Driel, P.B. a. A., van der Vorst, J.R., Verbeek, F.P.R., Oliveira, S., Snoeks, T.J.A., Keereweer, S., Chan, B., Boonstra, M.C., Frangioni, J.V., van Bergen en Henegouwen, P.M.P., Vahrmeijer, A.L., Lowik, C.W.G.M., 2014. Intraoperative fluorescence delineation of head and neck cancer with a fluorescent anti-epidermal growth factor receptor nanobody. Int. J. Cancer 134, 2663–2673. doi:10.1002/ijc.28601

Varache, M., Ciancone, M., Caputo, F., Laffont, C., Escudé, M., Jary, D., Boisseau, P., Texier, I., Navarro, F., Couffin, A.-C., 2016. Development and validation of characterization methods for lipidots® multifunctional platform: A step towards industrial transfer. Adv. Mater. - TechConnect Briefs 2016 1, 29–32.

West, W., Pearce, S., 1965. The Dimeric State of Cyanine Dyes. J. Phys. Chem. 69, 1894–1903. doi:10.1021/j100890a019

Wittenberg, N.J., Haynes, C.L., 2009. Using nanoparticles to push the limits of detection. Wiley Interdiscip. Rev. Nanomed. Nanobiotechnol. 1, 237–254. doi:10.1002/wnan.19

Wolfbeis, O.S., 2015. An overview of nanoparticles commonly used in fluorescent bioimaging. Chem. Soc. Rev. 44, 4743–4768. doi:10.1039/c4cs00392f

Yi, X., Wang, F., Qin, W., Yang, X., Yuan, J., 2014. Near-infrared fluorescent probes in cancer imaging and therapy: an emerging field. Int. J. Nanomedicine 9, 1347–1365. doi:10.2147/IJN.S60206

Yuan, A., Qiu, X., Tang, X., Liu, W., Wu, J., Hu, Y., 2015. Self-assembled PEG-IR-780-C13 micelle as a targeting, safe and highly-effective photothermal agent for in vivo imaging and cancer therapy. Biomaterials 51, 184–193. doi:10.1016/j.biomaterials.2015.01.069

Yuan, L., Lin, W., Zheng, K., He, L., Huang, W., 2013. Far-red to near infrared analyte-responsive fluorescent probes based on organic fluorophore platforms for fluorescence imaging. Chem. Soc. Rev. 42, 622–661. doi:10.1039/C2CS35313J

Yue, C., Liu, P., Zheng, M., Zhao, P., Wang, Y., Ma, Y., Cai, L., 2013. IR-780 dye loaded tumor targeting theranostic nanoparticles for NIR imaging and photothermal therapy. Biomaterials 34, 6853–6861. doi:10.1016/j.biomaterials.2013.05.071

Zhang, C., Liu, T., Su, Y., Luo, S., Zhu, Y., Tan, X., Fan, S., Zhang, L., Zhou, Y., Cheng, T., Shi, C., 2010a. A near-infrared fluorescent heptamethine indocyanine dye with preferential tumor accumulation for in vivo imaging. Biomaterials 31, 6612–6617. doi:10.1016/j.biomaterials.2010.05.007

Zhang, C., Wang, S., Xiao, J., Tan, X., Zhu, Y., Su, Y., Cheng, T., Shi, C., 2010b. Sentinel lymph node mapping by a near-infrared fluorescent heptamethine dye. Biomaterials 31, 1911–1917. doi:10.1016/j.biomaterials.2009.11.061

Zhegalova, N.G., He, S., Zhou, H., Kim, D.M., Berezin, M.Y., 2014. Minimization of self-quenching fluorescence on dyes conjugated to biomolecules with multiple labeling sites via asymmetrically charged NIR fluorophores. Contrast Media Mol. Imaging 9, 355–362. doi:10.1002/cmmi.1585

Figure 1

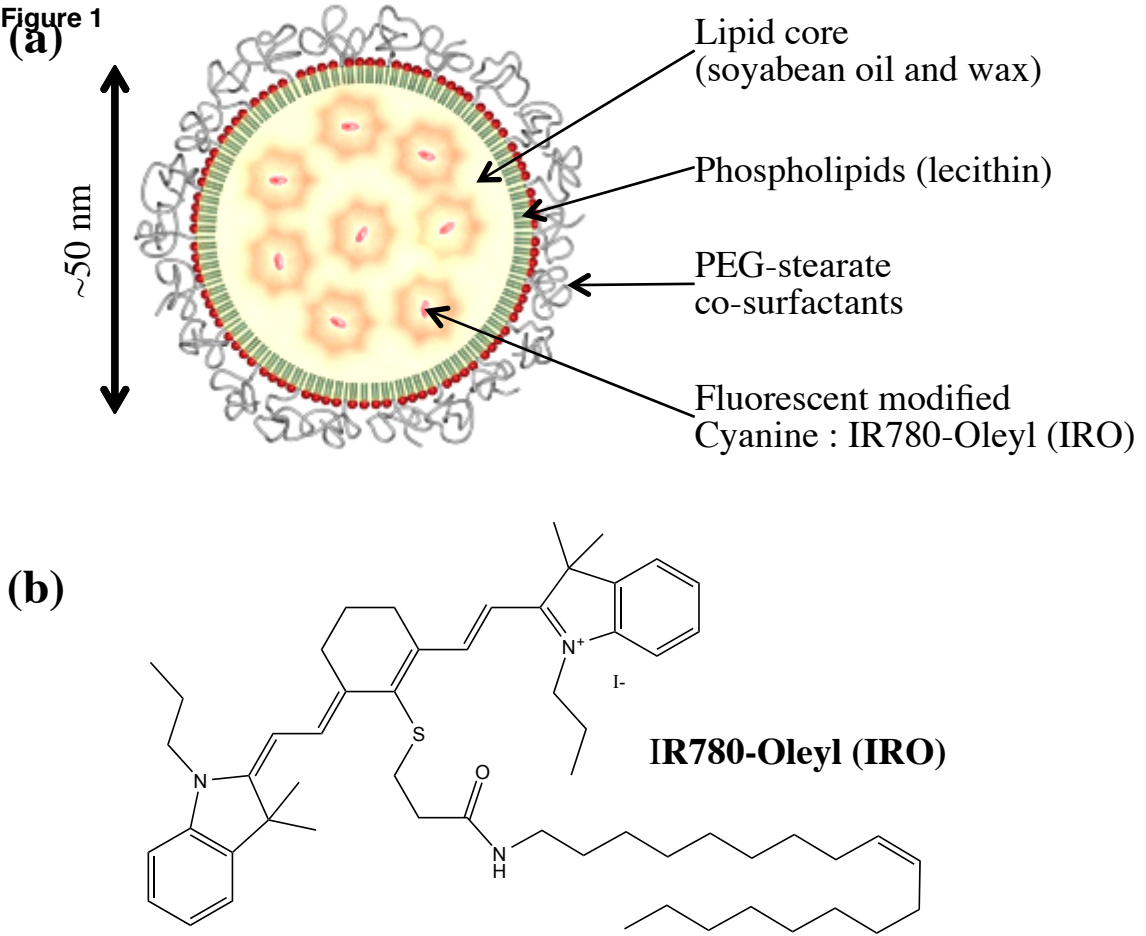
(a)
~50 nm
Lipid core
(soyabean oil and wax)
Phospholipids (lecithin)
PEG-stearate
co-surfactants
Fluorescent modified
Cyanine : IR780-Oleyl (IRO)
(b)
I-
S
O
N
H
IR780-Oleyl (IRO)

Figure 2

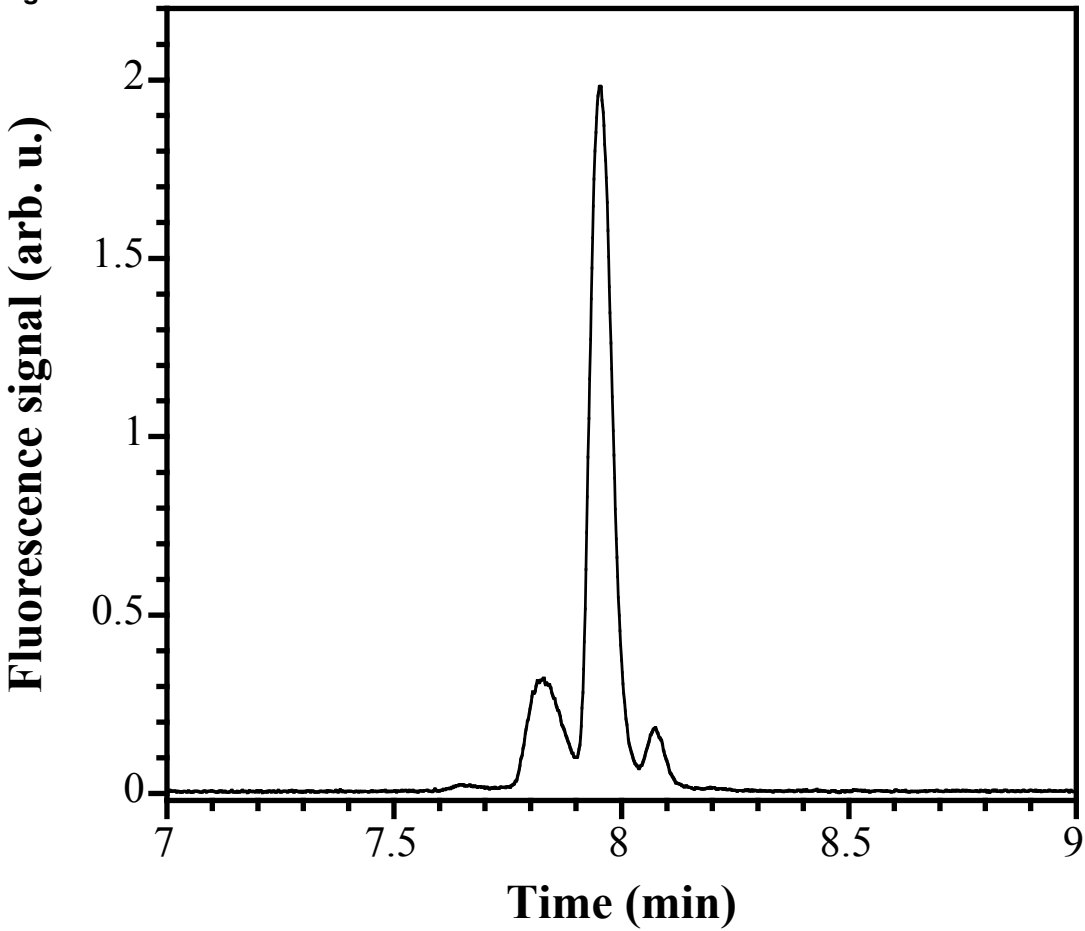

Figure 3

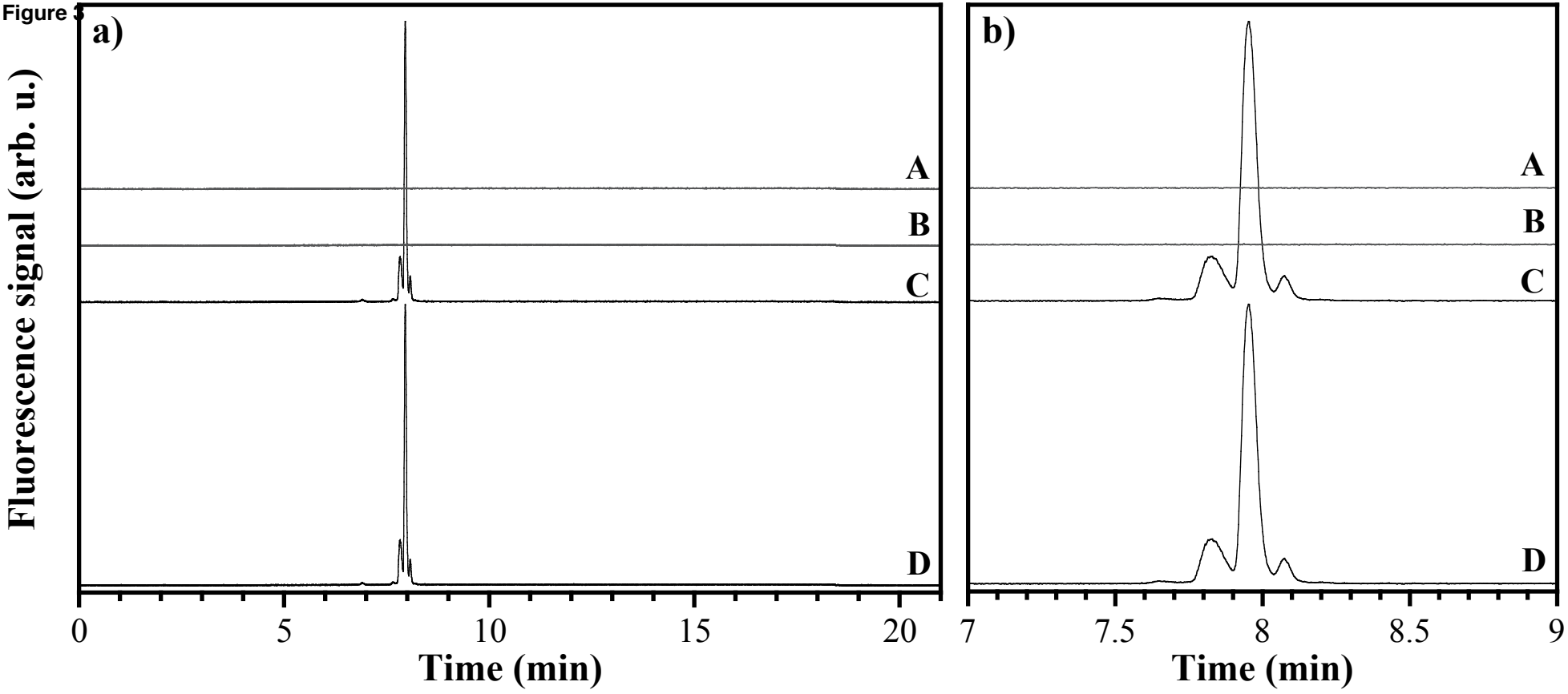
a)
b)
A
B
C
D
Fluorescence signal (arb. u.)
0
5
10
15
20
7
7.5
8
8.5
9
Time (min)
Time (min)

Figure 4

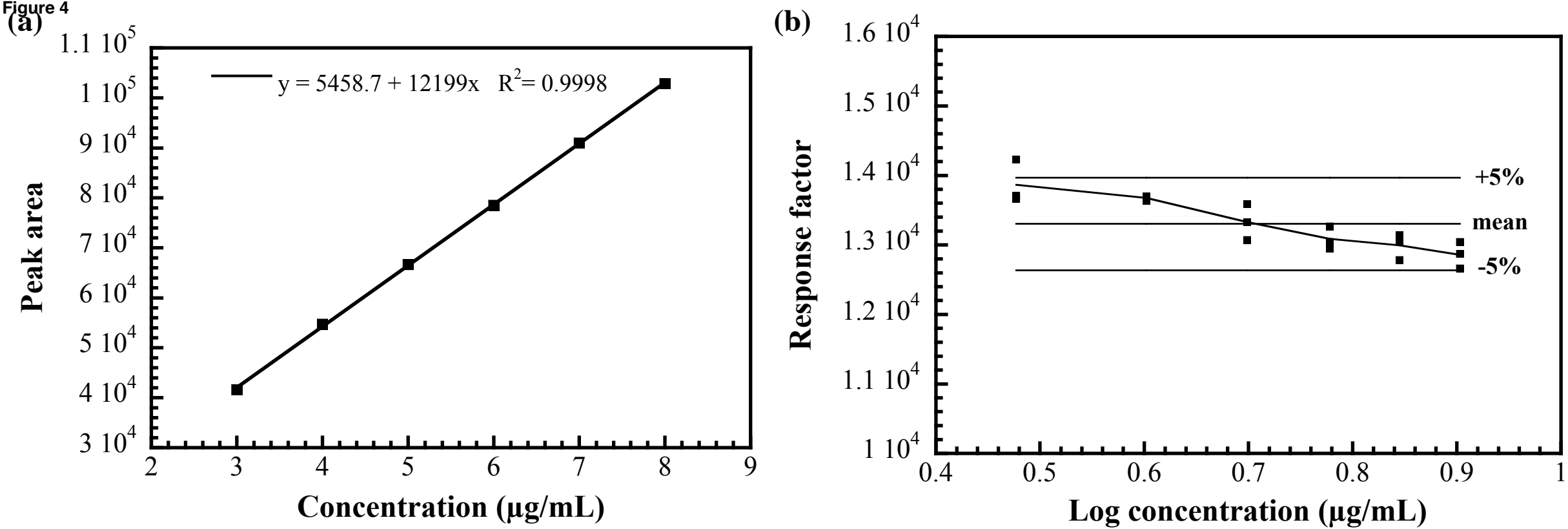
(a)
y = 5458.7 + 12199x R2= 0.9998
Peak area
Concentration (µg/mL)
(b)
Response factor
+5%
mean
-5%
Log concentration (µg/mL)

Figure 5

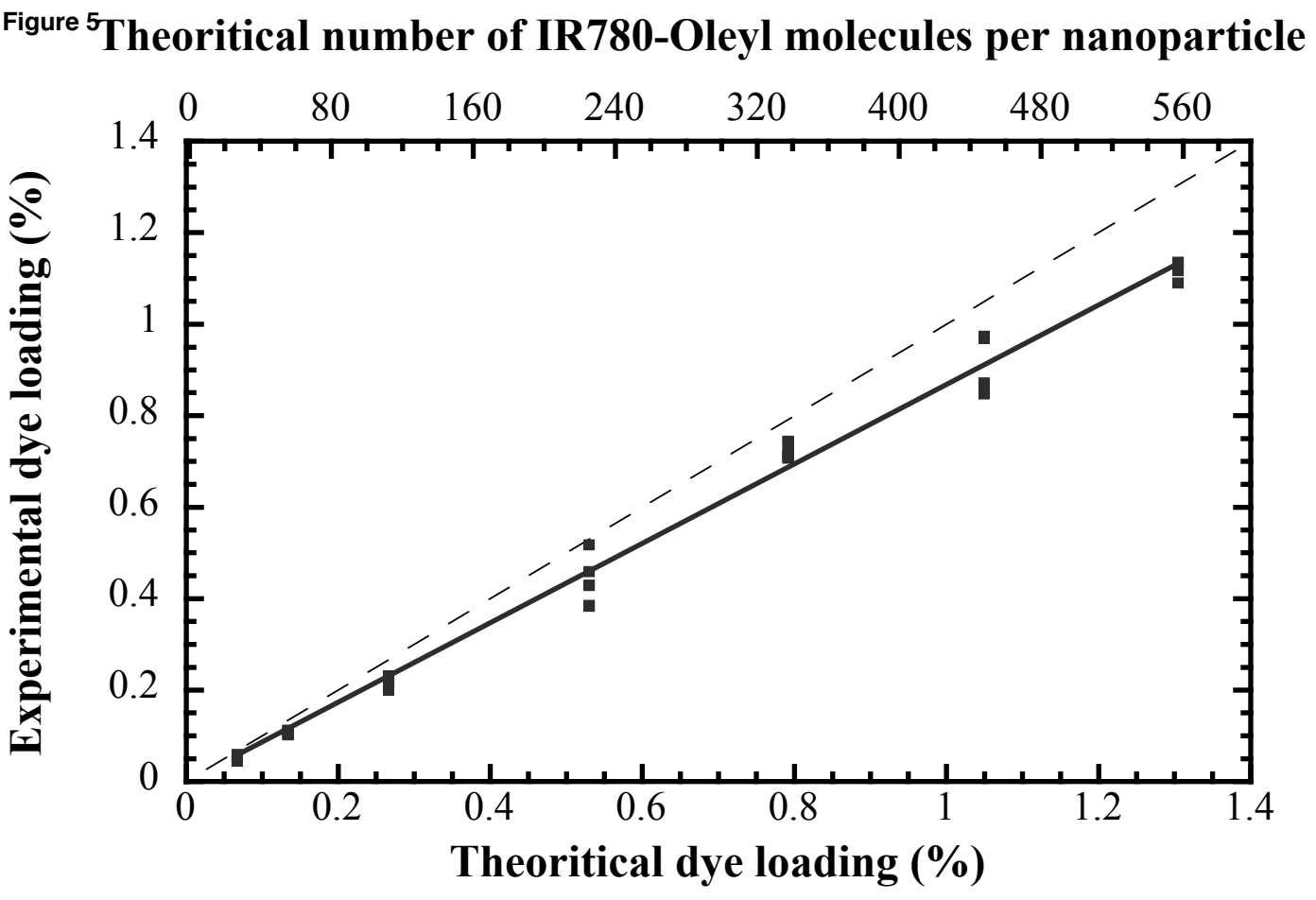
Theoritical number of IR780-Oleyl molecules per nanoparticle
0
80
160
240
320
400
480
560
Experimental dye loading (%)
1.4
1.2
1
0.8
0.6
0.4
0.2
0
0
0.2
0.4
0.6
0.8
1
1.2
1.4
Theoritical dye loading (%)

Figure 6

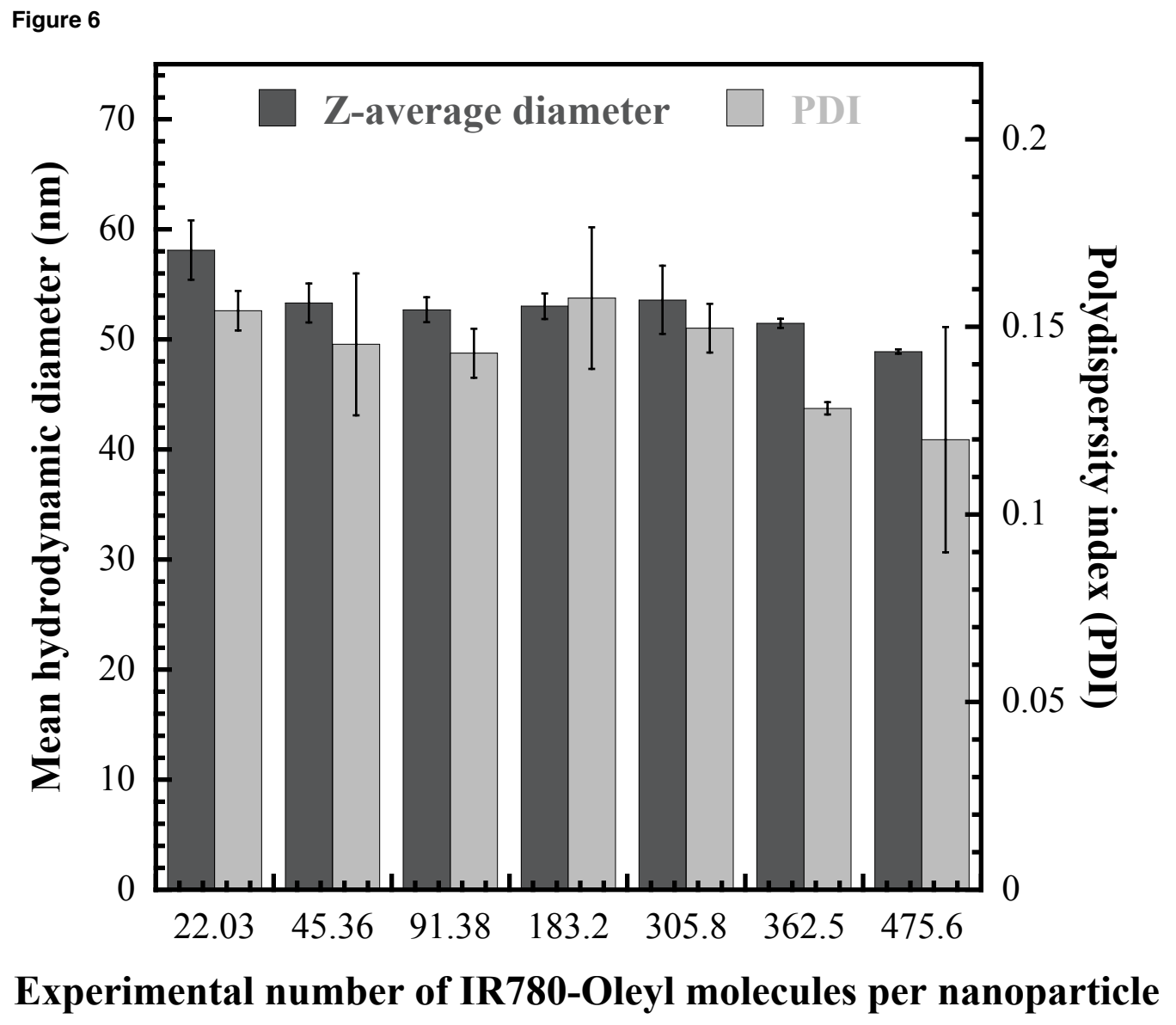
Z-average diameter
PDI
Mean hydrodynamic diameter (nm)
Polydispersity index (PDI)
0
10
20
30
40
50
60
70
0
0.05
0.1
0.15
0.2
22.03
45.36
91.38
183.2
305.8
362.5
475.6
Experimental number of IR780-Oleyl molecules per nanoparticle

Figure 7

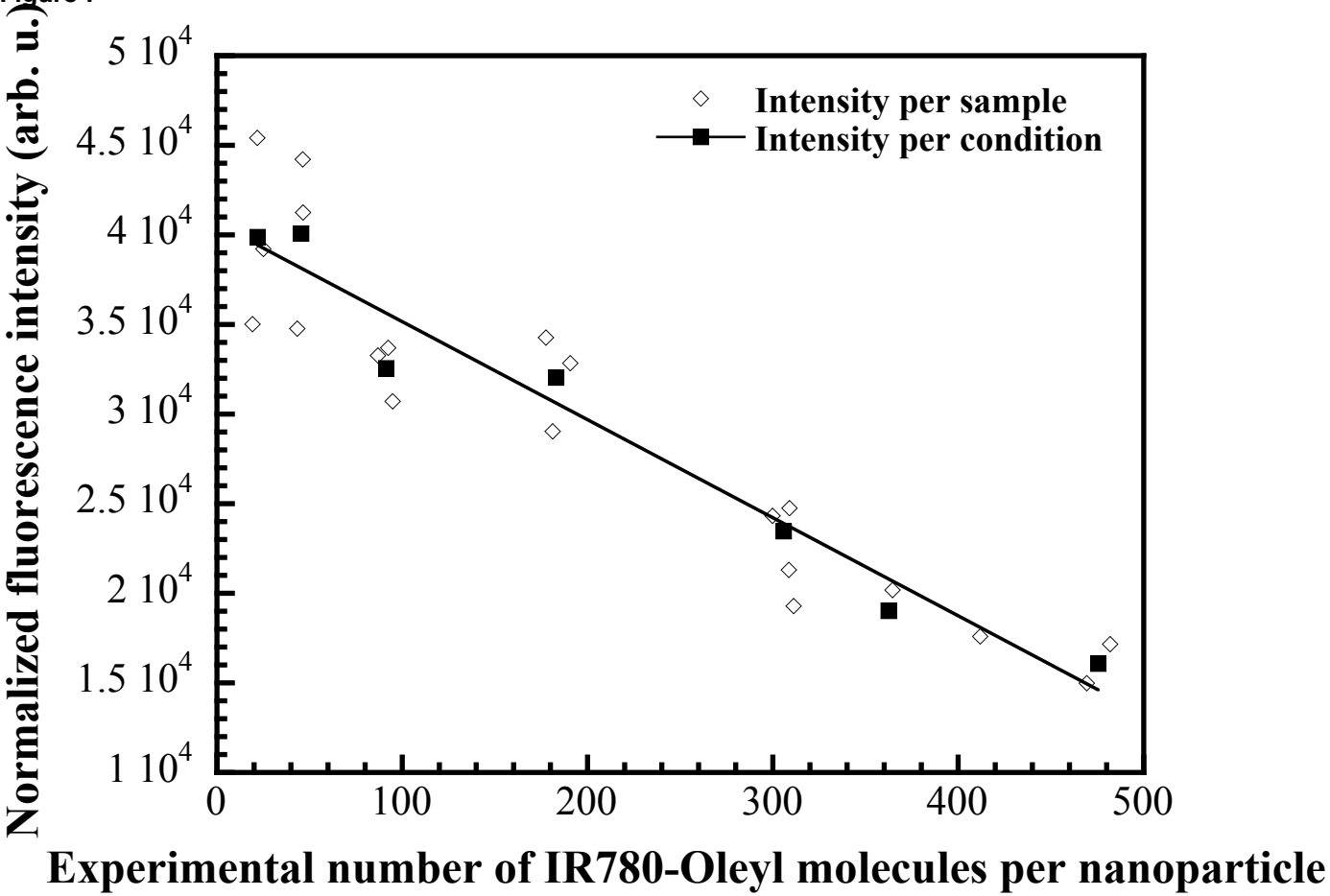
Normalized fluorescence intensity (arb. u.)
5 10^4
4.5 10^4
4 10^4
3.5 10^4
3 10^4
2.5 10^4
2 10^4
1.5 10^4
1 10^4
0
100
200
300
400
500
Intensity per sample
Intensity per condition
Experimental number of IR780-Oleyl molecules per nanoparticle

Figure 8

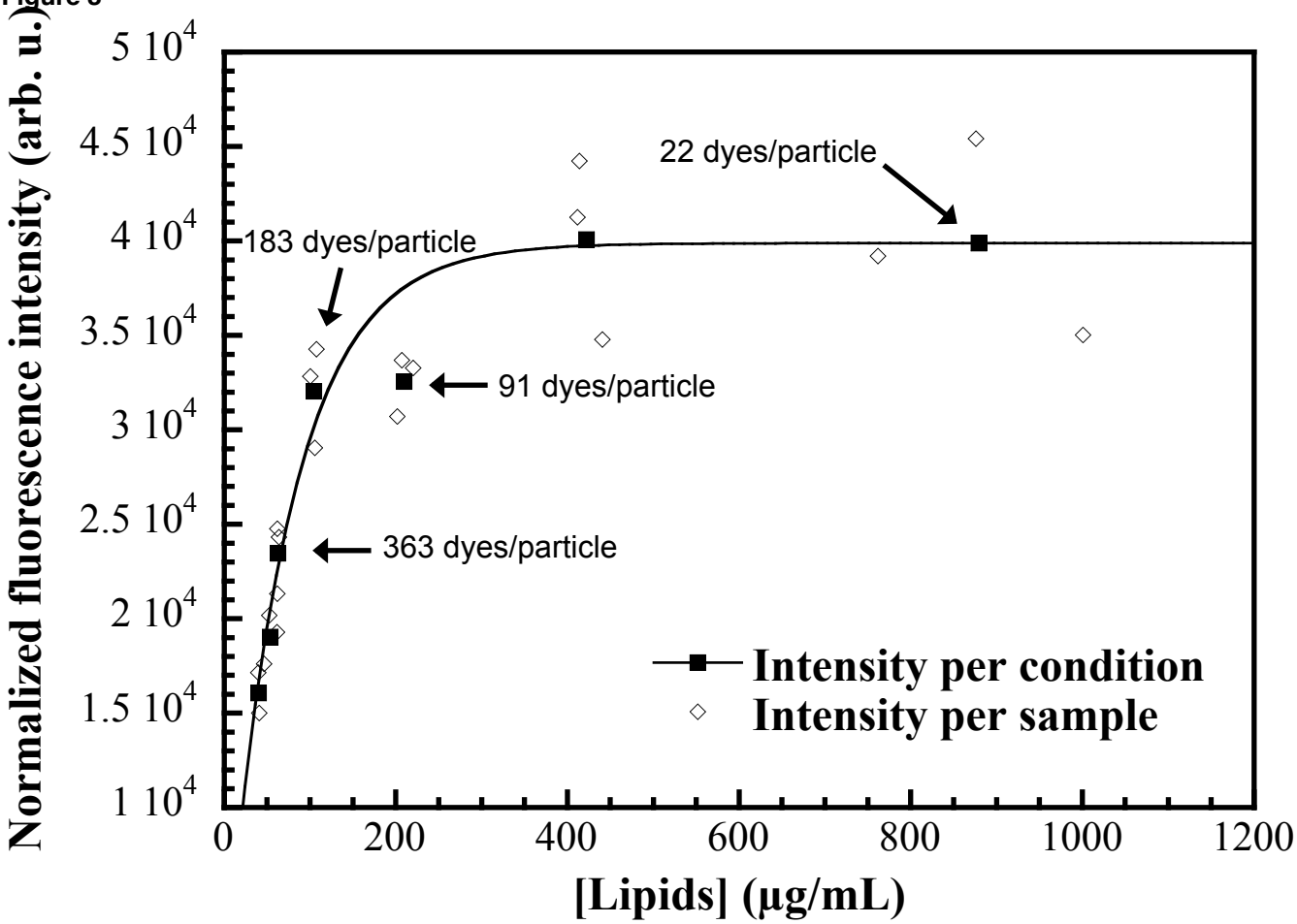
Normalized fluorescence intensity (arb. u.)
5 10^4
4.5 10^4
4 10^4
3.5 10^4
3 10^4
2.5 10^4
2 10^4
1.5 10^4
1 10^4
0
200
400
600
800
1000
1200
[Lipids] (µg/mL)
22 dyes/particle
183 dyes/particle
91 dyes/particle
363 dyes/particle
Intensity per condition
Intensity per sample